# State-selective chirped adiabatic passage on dynamically laser-aligned molecules

S. Thomas, S. Guérin,* and H. R. Jauslin
*Laboratoire de Physique, UMR 5027 CNRS, Université de Bourgogne, BP 47870, 21078 Dijon, France*
(Received 30 July 2002; published 3 January 2005)

We show that rovibrational state selectivity can be achieved by chirped adiabatic passage of molecules that are *adiabatically aligned* by a nonresonant laser field. We develop the tools to design the appropriate frequency and amplitude modulations that allow us to select a given route in the Hilbert space that leads to a final complete excitation of the chosen state, by infrared or by Raman processes. This method allows us to select a given vibrational state in a well-defined rotational $J$ state.

DOI: 10.1103/PhysRevA.71.013402 PACS number(s): 42.50.Hz, 32.80.Bx, 32.80.Lg

## I. INTRODUCTION

Selective excitation of the states of atoms and molecules by laser pulses is of considerable importance for the control of processes involving internal and external degrees of freedom [1,2].

A very promising method is the adiabatic passage by sweeping the laser frequency (chirping), which is robust with respect to variations of the field amplitude and frequency. This type of adiabatic passage can be induced by a one-photon infrared chirp [3] or by a Raman chirp [4]. The chirping technique is nowadays well developed in femto- and picosecond time scales (see, e.g., Ref. [5]). The vibrational excitation by adiabatic passage has been widely studied theoretically for models that do not include rotation (e.g., in Refs. [3], [4], [6], and [7]). It is well known that if one uses picosecond chirped pulses, the population is in general spread into a set of rotational states [8–10] due to the nanosecond time scale of the rotational motion. Only for very light molecules (such as $H_2$ and HF) this rotational time scale is of the order of picoseconds and the rovibrational selectivity can be achieved (see, for instance, Ref. [11], where nonrobust multiphoton $\pi$ pulses on a picosecond time scale have been used and Ref. [12] for rotational branching in $H_2$ by Raman chirped adiabatic passage). A rotational model that includes the spontaneous Raman processes has recently been studied [13].

On the other hand, alignment of molecules in their ground vibronic state by laser-induced adiabatic transport along *the pendular dressed states* can be achieved in general during nanosecond time scales [14–17]. This approach needs a strong nonresonant linearly polarized laser field which couples the rotational states (of rotational constant $B_0$) of the ground vibronic state by two-photon Raman processes through its anisotropic polarizability $\Delta\alpha$. One considers the molecular population initially in the rotational state $|J=0\rangle$, with projection $M=0$ of the rotational angular momentum along the field axis (which is a constant of motion). This leads to an effective rigid rotor dressed by a double-well potential whose minima are in the directions of the field polarization. The wells are deeper and thinner for a stronger field. The eigenvectors of the dressed Hamiltonian are called *pendular states*. Their associated eigenenergies (labeled by a positive integer $\tilde{J}$) as a function of the field amplitude form curves that are continuously connected to the energies associated to the bare states $|J\rangle$. They form two families (even and odd $\tilde{J}$) of near-degenerate eigenvalues. The lowest ones are well localized in the wells and correspond thus to molecular alignment. When the laser field is turned on slowly with respect to the two-photon detuning $6B_0/\hbar$ between the states $|J=2\rangle$ and $|J=0\rangle$, i.e., when [15]

$$6B_0/\hbar \gg 1/T_a, \tag{1}$$

with $T_a$ the duration of the aligning laser pulse, the dressed molecule is *adiabatically* carried along the pendular state $|\tilde{J}=0\rangle$.

In this paper, we show for a model including the vibration and rotation that we can selectively populate a given rovibrational state by chirped adiabatic passage while the molecule is dynamically aligned by an additional nanosecond laser. The mechanism we propose is as follows: The molecule is first adiabatically aligned by a nanosecond pulse. When this pulse is at its maximum, one uses picosecond chirped adiabatic passage to transfer the population to the excited pendular vibrational state, which is adiabatically reconnected to the desired vibrational state when the aligning nanosecond pulse falls down.

A classical-mechanical interpretation could lead to the idea that a well aligned molecule along a given axis would not be subjected to rotation and that the rotational structure could be consequently neglected from the model. We give below a precise quantum-mechanical formulation of this statement.

We develop a systematic procedure to design the appropriate pulse parameters (frequency and amplitude) to achieve the complete transfer to a given allowed rovibrational state. This procedure is based on the topology of the dressed energies as a function of the pulse parameters. It allows us to identify qualitatively the various adiabatic ways to achieve the transfer [18]. The adiabatic passage is quantitatively optimized with the use of specific time-dependent pulse parameters.

We first develop the tools of vibrational selectivity on a rotationless model before considering the complete rovibra-

*Electronic address: Stephane.Guerin@u-bourgogne.fr

 

tional problem. We illustrate the mechanisms on the example of CO molecules.

## II. TOOLS FOR VIBRATIONAL SELECTIVITY BY ADIABATIC PASSAGE: ROTATIONLESS MODEL

In this section we apply the general tools reviewed in Ref. [18] for the vibrational selectivity by adiabatic passage induced by chirped laser fields in rotationless molecules. The rotational degree of freedom is considered in the next section. These tools are based on the adiabatic theorem which states that the dynamics follows approximately the instantaneous eigenvectors associated to eigenvalues continuously connected to the initial one when the Hamiltonian is perturbed sufficiently slowly. When this principle is extended to a quantum system (here a molecule) dressed by a laser field that is pulsed and whose frequency is swept, one has to consider the adiabatic transport, or the so-called adiabatic passage, along eigenvectors of the dressed system molecule + laser field (the so-called Floquet states) as functions of the envelope amplitude and of the instantaneous frequency of the field [6,7]. This leads to surfaces of associated eigenvalues (the so-called quasienergies) as functions of the two field parameters (amplitude and frequency). Inspection of the topology of the surfaces allows us (i) to analyze the various transfers that are permitted by adiabatic transport, and (ii) to design the appropriate laser parameters that will drive the dynamics to a desired state. This has been applied to atomic beam deflection [19], to population transfer in two- and three-level systems [20], and to the production of entangled states [21]. Paths that optimize the nonadiabatic losses have been identified in two-level systems: they correspond to level lines of the eigenenergy surfaces [22]. In this section we extend this study to multilevel systems and show the remarkable efficiency of the process along level lines.

Adiabatic passage is of great interest for state selectivity since it allows population transfers that are robust with respect to fluctuations of the field parameters and with respect to partial knowledge of the system, provided that resonant effects are taken into account. The key of robustness comes from the classification of topologically equivalent curves that connect the same states in the adiabatic limit. In order to study the surfaces of quasienergies, it is therefore generally sufficient to consider effective Hamiltonians that incorporate the resonances. We illustrate below these principles on a few vibrational states that are near-resonant with a chirped laser field.

### A. Model

We consider a one-mode vibrational potential $V(x)$ (e.g., the ground electronic state of a diatomic molecule), associated to the vibrational coordinate $x$, giving the vibrational Hamiltonian

$$H_0(x) = T_{\mathrm{vib}}(\partial_x) + V(x), \tag{2}$$

with $T_{\mathrm{vib}}$ the vibrational kinetic energy. We denote by $|n\rangle$ the eigenvectors of $H_0(x)$ associated to the eigenenergies $\hbar\omega_n$. The vibrational mode is coupled to a field of the form $\mathcal{E}(t)\cos[\phi(t)+\theta]$ (where the carrier oscillations and the envelope parts are considered independently) through $\mu_0(x)$, the dipole moment in the ground electronic state of the molecule (permanent dipole moment, nonzero for heteropolar molecule):

$$H(x,t,\phi(t)+\theta) = H_0(x) - \mu_0(x)\mathcal{E}(t)\cos[\phi(t)+\theta], \tag{3}$$

with the amplitude $\mathcal{E}(t)=\mathcal{E}_0\sqrt{\Lambda(t)}$, and $\mathcal{E}_0$, $\Lambda(t)$, $\phi(t)$, respectively, the peak amplitude, the shape (ranging between 0 and 1) of the field intensity, the time-dependent phase, and $\theta$ an additional constant phase (that is used to apply conveniently the Floquet theory). We have here considered that the field is linearly polarized, with the polarization axis parallel to the dipole moment of the rotationless molecule. The instantaneous Floquet (or quasienergy) operator characterizing the molecular Hamiltonian dressed by the field reads

$$\begin{aligned} K &= -i\hbar\omega_{\mathrm{eff}}(t)\frac{\partial}{\partial\theta} + H(x,t,\theta) \\ &= -i\hbar\omega_{\mathrm{eff}}(t)\frac{\partial}{\partial\theta} + H_0(x) - \mu_0(x)\mathcal{E}(t)\cos\theta, \end{aligned} \tag{4}$$

where the effective (also called instantaneous) frequency coincides to the derivative of the phase

$$\omega_{\mathrm{eff}}(t) \equiv \frac{d\phi}{dt}(t). \tag{5}$$

The operator $-i\hbar\omega_{\mathrm{eff}}(t)\,\partial/\partial\theta$ in Eq. (4) characterizes the laser photon field operator in the sense that it can be derived from the photon number associated to a cavity-quantized field when the field is taken outside the cavity in the free space and contains a large average number of photons [23]. Its eigenvectors are denoted by $|k\rangle$ where $k$ is a positive or negative integer that characterizes the relative number of photons with respect to its average. We remark that if we define a time-dependent frequency $\omega(t)$ as $\phi(t)\equiv\omega(t)t$, then the effective frequency reads $\omega_{\mathrm{eff}}(t)=\dot{\omega}(t)t+\omega(t)$, where $\dot{\omega}\equiv d\omega/dt$.

The quasienergy surfaces are formed by the eigenvalues of this Floquet Hamiltonian as functions of the parameters $\omega_{\mathrm{eff}}$ and $\mathcal{E}$. They can be calculated (at least numerically) for any given potential $V(x)$. One can label the Floquet eigenvectors as $|n;k\rangle$, associated to the quasienergies $\lambda_{n,k}$ with the indices $n$ and $k$, respectively, related to the free molecule $H_0(x)$ and to the photon field. The quasienergies can be arranged in zones of *quasidegenerate quasienergies*, associated to quasiresonance between the molecule and the field, that are periodic since we have $\lambda_{n,k+\ell}=\lambda_{n,k}+\ell\hbar\omega_{\mathrm{eff}}$ for any positive or negative integer $\ell$. For simplicity, one considers the $N+1$ lowest bound states $\{|0\rangle,|1\rangle,\ldots,|N\rangle\}$, associated to the energies $E_0<E_1<\cdots<E_N$ of a Morse potential coupled by a field whose effective frequency is one-photon near-resonant: $\hbar\omega_{\mathrm{eff}}\approx E_1-E_0\approx E_2-E_1\approx\cdots\approx E_N-E_{N-1}$. The effective Hamiltonian in the resonant approximation, that takes into account the one-photon near resonances of one Floquet zone, reads as a tridiagonal matrix:

$$H_{\text{eff}} = \frac{\hbar}{2}\begin{bmatrix} 0 & \Omega_{0,1} & 0 & \cdots & 0 \\ \Omega_{0,1} & 2\Delta_1 & \Omega_{1,2} & \ddots & \vdots \\ 0 & \Omega_{1,2} & 2\Delta_2 & \ddots & 0 \\ \vdots & \ddots & \ddots & \ddots & \Omega_{N-1,N} \\ 0 & \cdots & 0 & \Omega_{N-1,N} & 2\Delta_N \end{bmatrix}, \quad (6)$$

with

$$\Delta_n := \frac{E_n - E_0}{\hbar} - n\omega_{\text{eff}} = n[\omega_0 + (n+1)a - \omega_{\text{eff}}], \quad (7)$$

the Rabi frequency (assumed real and positive without loss of generality)

$$\Omega_{i,j} = -\mathcal{E}(t)\langle i|\mu_0|j\rangle/\hbar, \quad (8)$$

the (constant) anharmonicity

$$a := [(\omega_{n+1} - \omega_n) - (\omega_n - \omega_{n-1})]/2\hbar = -\hbar\omega_0^2/4D, \quad (9)$$

with $D$ the dissociation energy, and the frequency $\omega_0$ related to the energy of the Morse potential: $E_n = \hbar\omega_0(n+\frac{1}{2}) + \hbar a(n+\frac{1}{2})^2$, $n=0,\ldots,N$. This effective Hamiltonian is valid for moderate field intensities $\Omega_{i,j} \ll \omega_0$ (in practice not larger than $10^{13}$ W/cm$^2$ to avoid ionization), for small detunings and anharmonicity $|\Delta_n|, |a| \ll \omega_0$ and for $N$ significantly smaller than the total number of bound states.

This Hamiltonian can be technically obtained in the Floquet picture as follows: We apply the unitary resonant transformation $R(\theta) \equiv \text{diag}[1, e^{-i\theta}, \ldots, e^{-i(N-1)\theta}]$ to the Floquet operator which allows to write the resonant terms as $\theta$ independent plus a nonresonant $\theta$-dependent rest $V_2$:

$$R^\dagger(\theta)KR(\theta) = -i\hbar\omega_{\text{eff}}(t)\frac{\partial}{\partial\theta} + H_{\text{eff}} + V_2(\theta). \quad (10)$$

The resonant transformation $R(\theta)$ allows to dress the bare states $|0\rangle$ with 0 photon, $|1\rangle$ with minus one photon, $|n\rangle$ with minus $n$ photons, and so on. The state corresponding to a bare state $|n\rangle$ dressed by $k$ photons, when the field is off, reads $|n;k\rangle^{\mathcal{E}=0} = |n\rangle \otimes e^{ik\theta}$. The rest $V_2(\theta)$ contains terms, coupling the Floquet zones, that become of order $\mathcal{O}(\mathcal{E}^2)$ after the application of perturbation theory. Since they are perturbative, their highest-order effects can be incorporated as Stark shifts. However, in the range of intensities considered here, they can be neglected with respect to the coupling Rabi frequency in $H_{\text{eff}}$ which is of order $\mathcal{O}(\mathcal{E})$.

### B. Surfaces of quasienergy

Figure 1 displays the quasienergy surfaces $\lambda_{n,k}$ in units of $\hbar\omega_0$ connected to the three lowest vibrational states, as functions of the effective frequency $\omega_{\text{eff}}$ and the field amplitude $\mathcal{E}$ taken as independent parameters. We have chosen the CO molecule for which $a \simeq -6.033\times10^{-5}$ a.u. and $\omega_0 \simeq 0.009\,89$ a.u., using an *ab initio* dipole moment [24]. These surfaces show the different connectivities that are topologically allowed by adiabatic passage. The topology is determined by the resonances characterized by the crossings (labeled as A, B, and $A_2$) of the curves at $\mathcal{E}=0$ [corresponding to the crossings of the diagonal elements of Eq. (6)].

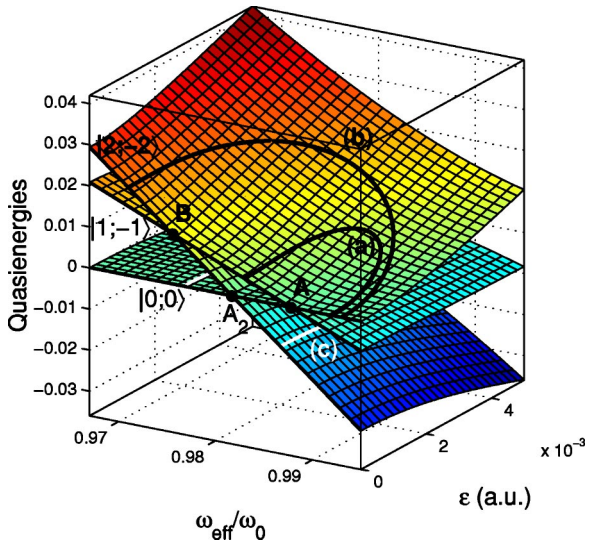


FIG. 1. (Color online) The first three quasienergy surfaces (in units of $\hbar\omega_0$), eigenvalues of $H_{\text{eff}}$ (6), as functions of the effective frequency (normalized by $\omega_0$) and the field amplitude $\mathcal{E}$ (in atomic units, with the correspondence amplitude-intensity $\mathcal{E}=5\times10^{-3}$ a.u. $\leftrightarrow I \approx 0.877$ TW/cm$^2$) calculated from the Hamiltonian (6) for the CO molecule. Paths (a) and (b) correspond to a transition from the state $|0\rangle$ to the states $|1\rangle$ and $|2\rangle$ with absorption of one and two photons, respectively, for decreasing frequency chirp. Path (c) corresponds to a transition from the state $|0\rangle$ to the state $|2\rangle$ with absorption of two photons for increasing frequency chirp.

Intersection A is determined by the crossing between the first and second diagonal elements which occurs at $\omega_{\text{eff}}^{(A)} = \omega_0 + 2a$, intersection B by the crossing between the second and third diagonal elements: $\omega_{\text{eff}}^{(B)} = \omega_0 + 4a$, and intersection $A_2$ by the crossing between the first and third diagonal elements: $\omega_{\text{eff}}^{(A_2)} = \omega_0 + 3a$. Thus the crossings A, B, and $A_2$ characterize, respectively, a one-photon resonance between the bare states $|0\rangle$ and $|1\rangle$, a one-photon resonance between $|1\rangle$ and $|2\rangle$, and a two-photon resonance between $|0\rangle$ and $|2\rangle$. For $\mathcal{E} \neq 0$, the crossings become avoided crossings. The labels $|0;0\rangle$, $|1;-1\rangle$, $|2;-2\rangle$ of Fig. 1 stand for the straight lines in the plane $\mathcal{E}=0$. The slope of these lines labeled by $|n;k\rangle$ corresponds to the relative number of photons: $\partial\lambda_{n,k}/\partial\omega_{\text{eff}}|_{\mathcal{E}=0}/\hbar = k$. Three topologically inequivalent paths are shown in Fig. 1 and give an insight into the state selectivity in this model. Path (a), going around crossing A, allows the population transfer from state $|0;0\rangle$ to $|1;-1\rangle$, i.e., the population transfer from the bare state $|0\rangle$ to $|1\rangle$ with absorption of one photon. Both paths (b) and (c) allow the population transfer from state $|0;0\rangle$ to $|2;-2\rangle$, i.e., the population transfer from the bare state $|0\rangle$ to $|2\rangle$ with absorption of two photons. Since path (b) goes around A and B, it can be described as a succession of two sequential one-photon processes. Since path (3) goes around $A_2$, it corresponds to a direct two-photon process.

### C. Optimization of population transfer using level lines

In addition to the topology, the success of adiabatic passage requires to find parameters that induce negligible nona-

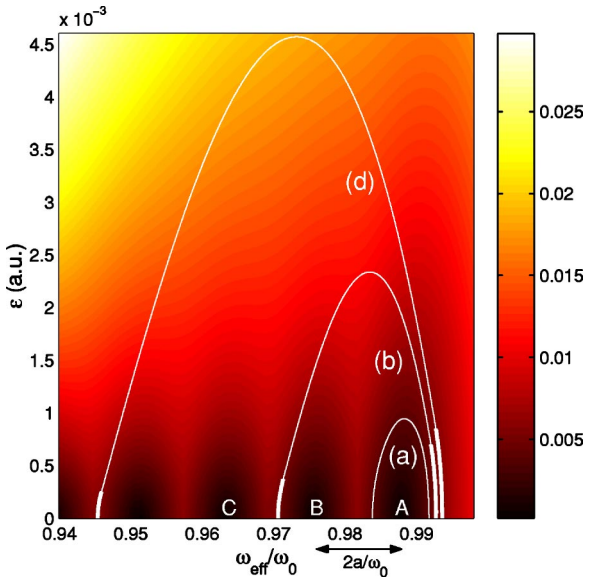


FIG. 2. (Color online) Contour plot of the distance between the upper closest neighbor surfaces of Fig. 1 as a function of the normalized effective frequency and the field amplitude $\mathcal{E}$. Paths (a) and (b) correspond to the ones of Fig. 1.

diabatic losses. The representation of the surfaces as contour plots of level lines allows to guide this search.

### 1. Sequential one-photon processes

Figure 2 shows the contour plot of the distance between the upper closest neighbor surfaces. Note that we have taken into account in this figure six states and six surfaces. The consecutive one-photon resonances at zero field corresponding to crossings appear in dark zones (one recovers intersections A and B). The crossings are separated at $2a/\omega_0$ in this diagram. For $\mathcal{E}=0$, the line at the right of intersection A corresponds to state $|0;0\rangle$; the segment between A and B corresponds to state $|1;-1\rangle$; the segment between B and C to state $|2;-2\rangle$ and so on for states $|n;-n\rangle$.

Optimal adiabatic passage which gives the minimal nonadiabatic loss for a given peak intensity and a smooth symmetric pulse shape has been shown to follow a level line for two-level systems [22]. This corresponds to parallel quasienergies at all times. This can be applied for population transfer from $|0\rangle$ and $|1\rangle$, using a level line that connects these two states. In this case, the only remaining parameter in the contour diagram is the detuning at the beginning of the process at time $t_i$: $\Delta_i \equiv \Delta_1(t=t_i)$. The additional condition that guarantees a negligible nonadiabatic loss can be expressed as

$$|\Delta_i| T \gg 1, \tag{11}$$

where $T$ is the characteristic duration of the pulse shape (that is given and assumed to be symmetric for simplicity). For a Gaussian pulse, $T$ can be taken as the full width at half maximum, and it has been shown in Ref. [22] that the condition (11) is more precisely $|\Delta_i| T \gg \sqrt{\ln 2}/2 \approx 0.42$ in this case. Figure 3 displays numerical simulations for a Gaussian pulse, which shows very efficient and monotonic population transfer already for $\Delta_i T = -2.7$.

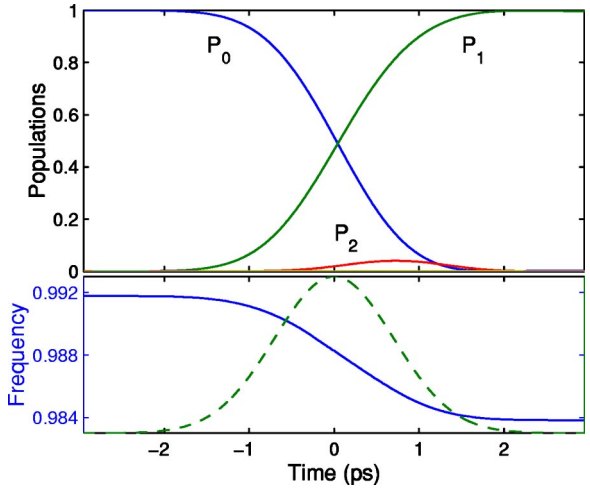


FIG. 3. (Color online) Numerical simulation of the probabilities $P_n = |\langle n|1\rangle|^2$ (upper frame) of the dynamics associated to the path (a) of Figs. 1 and 2 for a Gaussian intensity pulse shape $\Lambda(t) = e^{-4 \ln 2 (t/T)^2}$ (lower frame, dashed line) with $\Delta_i T \approx -2.7$, of peak intensity $I \approx 3.1 \times 10^{10}$ W/cm$^2$, and the associated effective frequency (lower frame, full line, in units of $\omega_0$).

Population transfer from $|0\rangle$ to states $|N>1\rangle$ cannot be achieved by the following of a single level line with a single pulse by the use of the contour of Fig. 2. One has to connect two pieces of level lines, one connecting the initial state, the other one connecting the final desired state. If the goal is to reach the state $|N\rangle$, one can choose as above $\Delta_i \equiv \Delta_1(t=t_i)$ such that $|\Delta_i| T \gg 1$ and $\Delta_f \equiv \Delta_N(t=t_f)$ at the final time $t_f$. One has to choose the way in which we leave and reach the level lines and a peak Rabi frequency. One can choose $\Delta_f = \Delta_i$. Adiabatic arguments impose to leave and reach the level lines as slowly as possible, which implies a peak Rabi frequency $\Omega_{\max} = \max_{n \le N, t} \Omega_{n-1,n}(t)$ such that $\Omega_{\max} > |\Delta_i|$. Figures 4 and 5 show numerics of population transfer to, respectively, the states $|2\rangle$ and $|4\rangle$. The success of the transfer requires a peak Rabi frequency larger than the one used for

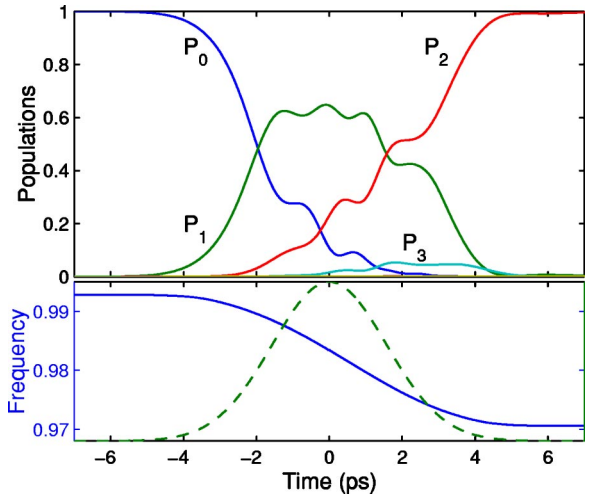


FIG. 4. (Color online) Same as Fig. 3 but with the dynamics associated to the path (b) of Figs. 1 and 2 with $\Delta_i T \approx -7.5$ and the peak intensity $I \approx 0.17 \times 10^{12}$ W/cm$^2$.

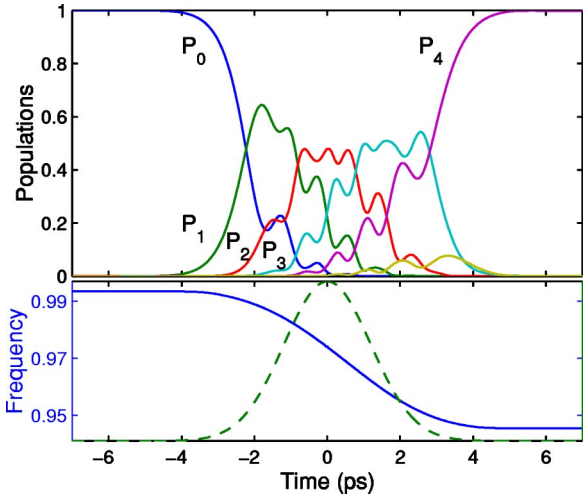


FIG. 5. (Color online) Same as Fig. 3 but with the dynamics associated to the path (d) of Fig. 2 with $\Delta_i T \approx -6.6$ and the peak intensity $I \approx 0.75 \times 10^{12}$ W/cm$^2$.

the single level line for the transfer to state $|1\rangle$. One notices that all the chirps designed for sequential one-photon processes with a Gaussian envelope have roughly the shape of a hyperbolic tangent curve.

### *2. Direct multiphoton processes*

Figure 1 shows that the path (c) corresponds to a direct two-photon process between the states $|0\rangle$ and $|2\rangle$, in the sense that it goes around the conical intersection $A_2$, the crossing between the first and third diagonal elements of the effective Hamiltonian (6). Figure 6 shows the contour plot of the distance between the two lowest surfaces of Fig. 1 around crossing $A_2$. One can see that level lines now connect

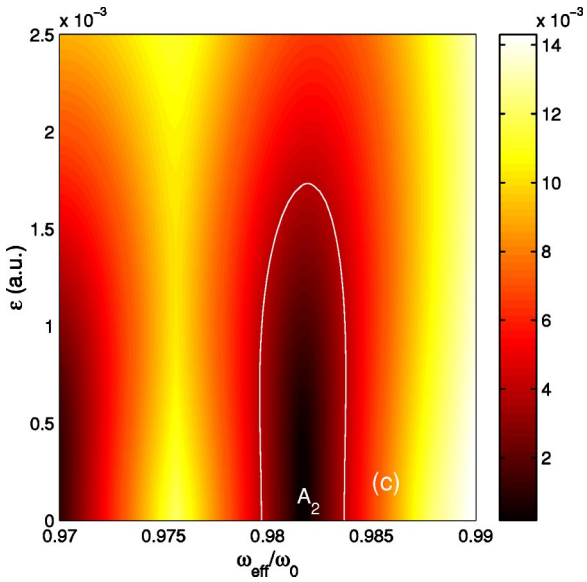


FIG. 6. (Color online) Contour plot of the distance between the lower closest neighbor surfaces of Fig. 1 as a function of the normalized effective frequency and the field amplitude $\mathcal{E}_0$. The paths (c) refer to the ones of Fig. 1.

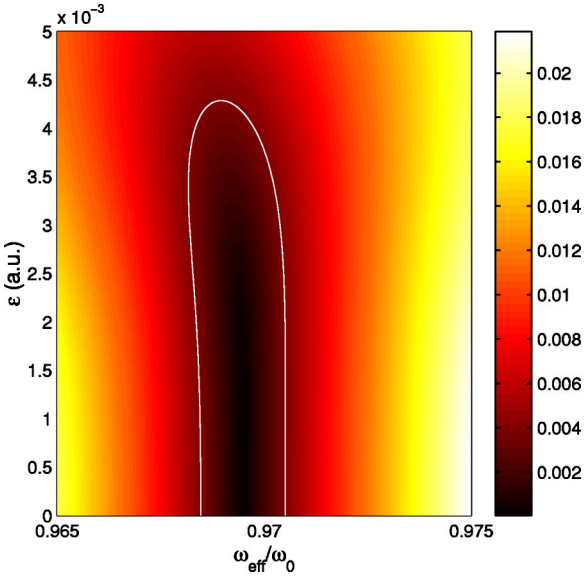


FIG. 7. (Color online) Contour plot of the distance between the two lower closest surfaces, connected to states $|1\rangle$ and $|5\rangle$ at zero field, as a function of the normalized effective frequency and the field amplitude $\mathcal{E}_0$. The white path is an example of a four-photon dynamics.

the states $|0\rangle$ and $|2\rangle$. One remarks that these level lines are slightly *bent*, due to the Stark shifts associated to this direct multiphoton process. Figure 7 shows the contour plot of the distance between the two lower closest surfaces, connected to states $|0\rangle$ and $|4\rangle$ at zero field, corresponding to a four-photon process between these states. The level lines are more bent for this high-order multiphoton process.

Figures 8 and 9 show numerics for population transfer to, respectively, states $|2\rangle$ and $|4\rangle$ by direct multiphoton adiabatic passage. One can see that the population transfer is monotonic unlike their counterparts obtained by sequential one-photon processes. It is more efficient in the sense that smaller duration and field amplitude is required to allow the

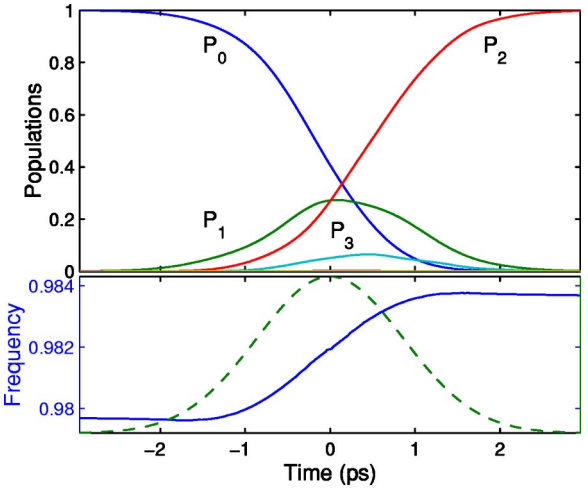


FIG. 8. (Color online) Same as Fig. 3 but with the dynamics associated to the path (c) of Figs. 1 and 6 with $\Delta_i T \approx 3.3$ and the peak intensity $I \approx 0.11 \times 10^{12}$ W/cm$^2$.

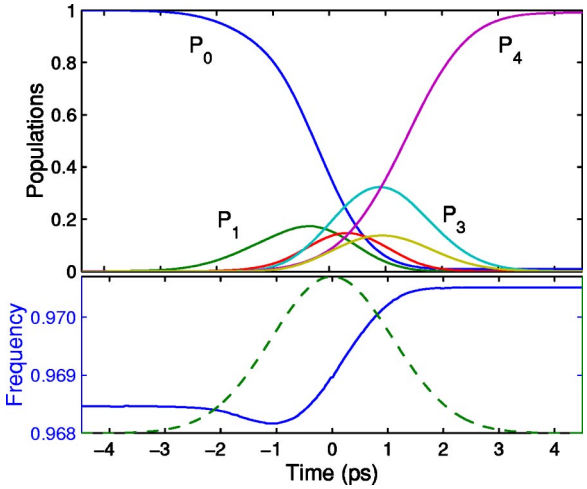


FIG. 9. (Color online) Same as Fig. 3 but with the dynamics associated to the path of Fig. 7 with $\Delta_i T \approx 4.2$ and the peak intensity $I \approx 0.64 \times 10^{12}$ W/cm$^2$.

transfer by adiabatic passage. This multiphoton process, however, requires in general a nonmonotonic chirp to follow the level line. We remark that numerical calculations for this multiphoton process include second order Stark shifts given by the diagonal (parallel) polarizability [see the diagonal of the Hamiltonian (14)]. The difference of the resulting calculations with and without this Stark effect is nonsignificant (less than 1%). This justifies to use here only the dominant one-photon resonant terms in the Hamiltonian (6).

The two different paths corresponding to the sequential process with twice one-photon and the direct two-photon process have been identified and experimentally tested between electronic atomic states in Ref. [25].

### D. Adiabatic passage by Raman chirping

We now investigate the selectivity of adiabatic passage by Raman chirping [4] using the topology tools. We assume that the frequencies of the pump and Stokes pulses of the Raman transitions are far detuned (low frequency) from any excited electronic states and also far detuned from any excited vibrational states. The Hamiltonian that has to be considered reads in this case (with both frequencies chirped)

$$H(x,t,\phi_P(t)+\theta_P,\phi_S(t)+\theta_S) = H_0(x) - \mu_0(x)\mathcal{E} - \frac{\alpha_\parallel(x)}{2}\mathcal{E}^2, \tag{12}$$

with $\alpha_\parallel(x)$ the polarizability parallel to the molecular axis, and the field decomposed in the pump (index $P$) and Stokes (index $S$) fields, of time-dependent phase, peak amplitude, and intensity pulse-shape, respectively, $\phi_j(t)$, $\mathcal{E}_{0j}$ and $\Lambda_j(t)$, $j=P,S$:

$$\mathcal{E} := \mathcal{E}_P(t)\cos[\phi_P(t)+\theta_P] + \mathcal{E}_S(t)\cos[\phi_S(t)+\theta_S], \tag{13}$$

$\mathcal{E}_P(t)=\mathcal{E}_{0P}\sqrt{\Lambda_P(t)}$, $\mathcal{E}_S(t)=\mathcal{E}_{0S}\sqrt{\Lambda_S(t)}$. The additional constant phases $\theta_P$ and $\theta_P$ allow a convenient formulation of the two-mode Floquet theory (see below). The effective Hamiltonian, that takes into account the Raman two-photon near resonances of one Floquet zone in the ground electronic state, is again a tridiagonal matrix:

$$H_{\text{eff}} = \hbar \begin{bmatrix} S_0 & \Omega_{0,1} & 0 & \cdots & 0 \\ \Omega_{0,1} & \Delta_1 + S_1 & \Omega_{1,2} & \ddots & \vdots \\ 0 & \Omega_{1,2} & \Delta_2 + S_2 & \ddots & 0 \\ \vdots & \ddots & \ddots & \ddots & \Omega_{N-1,N} \\ 0 & \cdots & 0 & \Omega_{N-1,N} & \Delta_N + S_N \end{bmatrix} \tag{14}$$

with in this case

$$\Delta_n := \frac{E_0 - E_n}{\hbar} + n\omega_{\text{eff}} = -n[\omega_0 + (n+1)a - \omega_{\text{eff}}], \tag{15}$$

the effective frequency

$$\omega_{\text{eff}}(t) \equiv \frac{d\phi_P}{dt}(t) - \frac{d\phi_S}{dt}(t), \tag{16}$$

the Rabi frequency

$$\Omega_{i,j} = -\mathcal{E}_P(t)\mathcal{E}_S(t)\langle i|\alpha_\parallel|j\rangle/\hbar, \tag{17}$$

and the relative Stark shifts

$$S_i = -[\mathcal{E}_P^2(t) + \mathcal{E}_S^2(t)]\langle i|\alpha_\parallel|i\rangle/\hbar. \tag{18}$$

It is a good approximation to use the static polarizabilities instead of the dynamical ones when the frequencies are far red detuned from any excited electronic states (i.e., low frequencies with respect to the electronic states).

We obtain technically this effective Hamiltonian starting with the two-mode Floquet Born-Oppenheimer Hamiltonian,

$$K = -i\hbar\omega_P(t)\frac{\partial}{\partial\theta_P} - i\hbar\omega_S(t)\frac{\partial}{\partial\theta_S} + H(x,t,\theta_P,\theta_S), \tag{19}$$

which itself results from a static perturbation theory of the full field+molecule (whose axis is assumed parallel to the field polarization) with respect to the electronic coordinates, in the Born-Oppenheimer approximation, up to the second order in field amplitude [18]. We take into account the contribution of the excited electronic states through the parallel polarizability $\alpha_\parallel(x)$ by applying the unitary resonant transformation $R := \text{diag}[1, e^{i(\theta_S-\theta_P)}, \ldots, e^{i(N-1)(\theta_S-\theta_P)}]$, which allows us to write

$$R^\dagger K R = -i\hbar\omega_P\frac{\partial}{\partial\theta_P} - i\hbar\omega_S\frac{\partial}{\partial\theta_S} + H_{\text{eff}} + O(\mathcal{E}_{P,S}^3). \tag{20}$$

In this Raman process with the use of frequencies far blue detuned between vibrational states (e.g., with visible light), the vibrational contribution to the Stark shifts and to the coupling is generally negligible compared to the electronic contribution. The resulting effective Hamiltonian (14) does not depend on the values of the field frequencies as a first approximation.

The tools presented in the preceding subsections can be applied for the selectivity by Raman chirping. The results will be very similar both for sequential Raman two-photon

processes as for direct higher multiphoton processes (such as four,six,… photon processes), since the effective Hamiltonian (14) has the same form as Eq. (6) apart from additional non-negligible Stark shifts, that will bend the level lines of the contour plots of differences of quasienergy surfaces. This will lead in general to a nonmonotonic chirping for efficient following of level lines.

## III. ROVIBRATIONAL SELECTIVITY BY ADIABATIC PASSAGE OF AN ADIABATICALLY ALIGNED MOLECULE

In this section we consider the complete rovibrational molecule, and the state selectivity when the molecule is adiabatically aligned. More precisely, we first adiabatically align the molecule with a nonresonant linear polarized nanosecond pulse, apply next a picosecond chirped field that will transfer the population among the resulting dressed vibrational pendular states, and finally switch off the aligning laser adiabatically to reconnect the bare rovibrational states. We first analyze the selection rules of the vibrational pendular states, show the different possibilities of climbing, and construct the Hamiltonian of the model. We next present the state selectivity scenario by one-photon infrared and Raman chirpings.

### A. Conditions of selectivity

One considers that the rovibrational structure of the molecule is made as a first approximation of uncoupled rigid rotors (of respective rotational constants $B_v$), one for each vibrational state $v=0,1,\ldots$. The effective Hamiltonian associated to an isolated vibration $v$ of the molecule dressed by a nonresonant aligning laser of amplitude $\mathcal{E}_a$ reads in the high-frequency limit (with respect to the rotational structure) [14,26]

$$H_{vv}^{\mathrm{nr}} = B_v J^2 + \mathcal{E}_a^2(\Delta\alpha_{vv}\sin^2\Theta - \alpha_{\parallel,vv})/4, \tag{21}$$

with $\Theta$ the polar angle between the molecular axis and the direction of the nonresonant field, $\Delta\alpha_{v'v}=\alpha_{\parallel,v'v}-\alpha_{\perp,v'v}$, $\alpha_{\perp,v'v}=\langle v'|\alpha_{\perp}|v\rangle$, $\alpha_{\parallel,v'v}=\langle v'|\alpha_{\parallel}|v\rangle$. $J$ is the angular momentum. It consists then of *an effective double well potential for each vibrational state*. The central point is that for an ideally strong aligning field, the pendular eigenenergies of each effective double well potential have a structure of two families labeled by even and odd $J$, of *doubly near-degenerate pendular ladders* of *large* spacing $E_{v,\tilde{J}+2}-E_{v,\tilde{J}}\sim 2\,(\mathcal{E}_a\sqrt{\Delta\alpha B_v}-B_v\tilde{J})$ [14], which become approximately harmonic $\hbar\omega_v^{(\mathrm{rot-alig})}\sim 2\mathcal{E}_a\sqrt{\Delta\alpha B_v}$ for large amplitude $\mathcal{E}_a$ and low $\tilde{J}$. This is shown in Fig. 10 which displays the pendular energies as a function of the dimensionless quantity characterizing the alignment efficiency

$$\gamma_a = \mathcal{E}_a^2\Delta\alpha_{00}/4B_0. \tag{22}$$

As expected, we can observe for increasing $\gamma_a$ the states $|\tilde{J}=2k\rangle$ and $|\tilde{J}=2k+1\rangle$, $k=0,1,2,\ldots$, becoming near degenerate by pairs and the formation of an harmonic ladder for the lowest $\tilde{J}$ of increasing spacing.

If one considers infrared one-photon dipolar transitions (for heteronuclear molecules), the selection rules are $\Delta\tilde{J}=\pm1,\pm3,\pm5,\ldots$ [14] with $\Delta v=\pm1$ (if one assumes $B_{v+1}\approx B_v$). For a picosecond chirping applied while the molecule is dynamically aligned, in the ideal situation of a very efficient alignment with infinite spacings $\hbar\omega_v^{(\mathrm{rot-alig})}$, the climbing of the vibrational ladder would occur following the sequence with alternating $\tilde{J}=0$ and $\tilde{J}=1$. We would obtain the following sequence, considering the states at the end of the pulses: $|v=0,J=0\rangle\rightarrow|v=1,J=1\rangle\rightarrow|v=2,J=0\rangle\rightarrow|v=3,J=1\rangle\rightarrow\ldots$, which is the one one would obtain in the rotationless model. The same arguments can be applied for a Raman chirping, with selection rules $\Delta\tilde{J}=0,\pm2,\pm4,\ldots$ and $\Delta v=0,\pm1$, which gives for $\Delta v=\pm1$ the climbing sequence with the same $\tilde{J}$: $|v=0,J=0\rangle\rightarrow|v=1,J=0\rangle\rightarrow|v=2,J=0\rangle\rightarrow\ldots$.

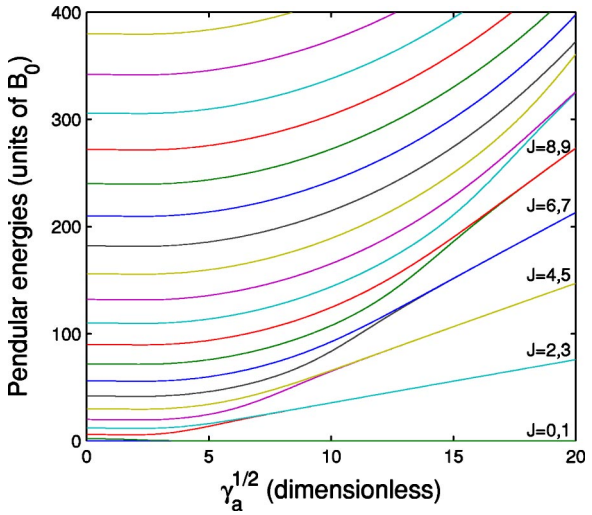


FIG. 10. (Color online) First lowest pendular energies $E_{\tilde{J}}-E_{\tilde{J}=0}$ of the ground vibronic state as functions of $\sqrt{\gamma_a}$ for a nonresonant field. The values of $J$ indicate the connection of the lines when $\gamma_a=0$.

However, the study of a concrete situation requires an aligning nanosecond laser pulse of peak intensity not larger than $10^{13}$ W/cm$^2$ to avoid ionization. This peak intensity gives an upper limit for the spacing $\hbar\omega_0^{(\mathrm{rot-alig})}$ of the pendular double harmonic ladder, that has to be characterized. Achieving the rovibrational climbing requires to prevent the rotational spreading, which is possible when the field amplitude satisfies

$$2\mathcal{E}_a\sqrt{\Delta\alpha B_0}/\hbar \gg 1/T_c, \tag{23}$$

where $T_c$ is the pulse duration of the chirped picosecond pulse (the full width half maximum for Gaussian pulses). For instance, for CO, we have $2\sqrt{\Delta\alpha B_0}/\hbar\approx 0.011$ a.u., which already requires $I_a\sim 10^{13}$ W/cm$^2$ for the intensity of the aligning field to satisfy the condition (23) with $T_c\sim 1$ ps. This condition has to be compared with the intrinsic condition [see Eq. (1)]

$$6B_0/\hbar \gg 1/T_c \tag{24}$$

required to avoid the rotational spreading in absence of aligning laser, which can be satisfied only for very light molecules in the picosecond regime of chirping [12]. The align-

ment can be well quantified by the observable $\langle\cos^2\Theta\rangle$, which reads in the strong-field limit [14]

$$\langle\cos^2\Theta\rangle \to 1 - 1/\sqrt{\gamma_a}. \tag{25}$$

This shows that satisfying the condition (23) will lead to a well aligned molecule $\langle\cos^2\Theta\rangle \sim 0.9$ for a typical rotational constant $B_0 \sim 1$ cm$^{-1}$ of linear molecules (we have for CO: $B_0 \approx 1.92$ cm$^{-1}$) and $T_c \sim 1$ ps. The use of a rotationless model with $\Theta = 0$ would be in this case a quite good approximation to study the vibrational climbing.

We use in the following a complete model for vibration and rotation to show the feasibility of the state selectivity of an aligned molecule. Four particular strategies can be implemented with such a model: (i) a one-photon chirped infrared scheme with an additional aligning nanosecond laser allowing to climb the vibrational ladder and to end in the isotropic state $J=0$ (for even $v$) or in $J=1$ (for odd $v$) at the end of the pulses: $|v=0,J=0\rangle \to |v=1,J=1\rangle \to |v=2,J=0\rangle \to |v=3,J=1\rangle \to |v=4,J=0\rangle \to \cdots$, and (ii) a chirped Raman scheme, with one of the two lasers acting also as the aligning nanosecond laser, allowing us to follow the particular sequences $|v=0,J=0\rangle \to |v=0 \text{ or } 1, J=0 \text{ or } 2\rangle \to |v=0 \text{ or } 2, J=0,2 \text{ or } 4\rangle \to |v=3,J=0,2,\ldots \text{or } 6\rangle \to |v=4,J=0,2,\ldots \text{or } 8\rangle \to \cdots$, i.e., at the end of the pulses (a) to climb the rotational ladder in the same $v$, (b) to climb the vibrational ladder and to end up in $J=0$, or (c) to climb the vibrational and rotational ladders.

### B. Model

The molecule is subjected to an aligning nonresonant field $\varepsilon_a(t)\cos(\omega_a t + \theta_a)$, of fixed carrier frequency $\omega_a$ and amplitude $\varepsilon_a(t) = \varepsilon_{0a}\sqrt{\Lambda_a(t)}$, and to a chirped field $\mathcal{E}_c(t)\cos(\phi_c(t) + \theta_c)$, of time-dependent phase $\phi_c(t)$ and amplitude $\mathcal{E}_c(t) = \mathcal{E}_{0c}\sqrt{\Lambda_c(t)}$. The peak amplitudes and the envelopes (taken as Gaussian) for the aligning and chirped fields are respectively denoted $\mathcal{E}_{0a}$, $\Lambda_a(t)$, $\mathcal{E}_{0c}$, $\Lambda_c(t)$. To construct the effective dressed Hamiltonian for the nonresonant aligning field, we will apply a high-frequency contact transformation [18,26] to the Born-Oppenheimer Floquet Hamiltonian,

$$\begin{aligned} K = &- i\hbar\omega_a\frac{\partial}{\partial\theta_a} - i\hbar\phi_c(t)\frac{\partial}{\partial\theta_c} + H_0(x,\Theta,\varphi) \\ &- \mu_0(x)[\mathcal{E}_a(t)\cos\theta_a + \mathcal{E}_c(t)\cos\theta_c]\cos\Theta \\ &+ [\Delta\alpha(x)\sin^2\Theta - \alpha_\parallel(x)]/2 \\ &\times [\mathcal{E}_a(t)\cos\theta_a + \mathcal{E}_c(t)\cos\theta_c]^2, \end{aligned} \tag{26}$$

where

$$H_0(x,\Theta,\varphi) \coloneqq T_{\text{vib}}(\partial_x) + B(x)T_{\text{rot}}(\Theta,\partial_\Theta,\partial_\varphi) + V(x), \tag{27}$$

with $\Theta$ the polar angle between the molecular axis and the direction of the linear polarized fields (in the same direction), $\varphi$ the azimuthal angle, $T_{\text{rot}}$ the rotational kinetic energy, $B$ the rotational constant, and $\Delta\alpha = \alpha_\parallel - \alpha_\perp$. $\alpha_\parallel$ and $\alpha_\perp$ are the static polarizabilities, respectively, parallel and perpendicular to the molecular axis (since we consider low frequencies with respect to the electronic states). We will consider $M=0$, which is invariant for linear polarized fields. We will next use the one-photon resonant approximation for the infrared chirp and the two-photon resonant approximation for the Raman chirp [18]. The effective Hamiltonian between vibrational blocks $H_{v'v} = \langle v'|H|v\rangle$, of energy $\hbar\omega_v$ and of rotational constant $B_v = \langle v|B|v\rangle$, reads thus [18,27]

$$H_{vv} = B_v J^2 + a_{vv}(\mathcal{E}_a^2 + \mathcal{E}_c^2) + \hbar\Delta_v(t), \tag{28a}$$

$$H_{v'\neq v} = -\hbar\Omega_{v'v}(t)/2, \tag{28b}$$

with (terms of second order in $1/\hbar\omega$ have been neglected)

$$a_{v'v} = (\Delta\alpha_{v'v}\sin^2\Theta - \alpha_{\parallel,v'v})/4, \tag{29}$$

where we have denoted $\mu_{0,v'v} = \langle v'|\mu_0|v\rangle$. The Stark shifts $a_{vv}(\mathcal{E}_a^2 + \mathcal{E}_c^2)$ allow the alignment of the molecule. The quantities $\mu_{0,v'v}$, $\alpha_{\perp,v'v}$, and $\alpha_{\parallel,v'v}$ have been calculated for the CO molecule from the *ab initio* calculations of Ref. [24]. For the one-photon infrared chirp, the Rabi frequencies read

$$\Omega_{v'v}(t) = \mu_{0,v'v}\mathcal{E}_c(t)\cos\Theta/\hbar, \tag{30}$$

and the detunings are $\Delta_v = \omega_v - \omega_0 - v\,d\phi_c/dt = v[\omega_0 + (v+1)a - d\phi_c/dt]$ [see Eq. (7)]. For the Raman process, one has

$$\Omega_{v'v}(t) = 2\mathcal{E}_a\mathcal{E}_c a_{v'v}/\hbar, \tag{31}$$

and $\Delta_v = \omega_0 - \omega_v + v(w_a - d\phi_c/dt) = -v[\omega_0 + (v+1)a - (\omega_a - d\phi_c/dt)]$ [see Eq. (15)].

### C. State selectivity by infrared chirping

Considering that the molecule is aligned, we can study the transfer by chirped adiabatic passage between the pendular vibrational states. This is done using the tools described in the preceding section: We consider the surfaces of the stationary dressed energies (of the aligned molecule) as a function of the two parameters: intensity and effective frequency of the chirped laser, and construct in this diagram the path connecting the initial state with the given final one (if the connection exists). This is well visualized using contour plots of differences of some surfaces. We show in Fig. 11, for the CO molecule, the contour plot of the difference of the closest neighboring surfaces, connected to $|v=0,\tilde{J}=0\rangle$, $|v=1,\tilde{J}=1\rangle$, $|v=2,\tilde{J}=0\rangle$, …, $|v=6,\tilde{J}=0\rangle$, $|v=7,\tilde{J}=1\rangle$ when the chirped field is off: $\mathcal{E}_c=0$. We can construct an appropriate path connecting the initial state $|v=0,J=0\rangle$ to a final chosen path. A path (a), as a level line, is shown to go from the vibrational pendular state $|v=0,\tilde{J}=0\rangle$ to $|v=1,\tilde{J}=1\rangle$. This path has been shown to be optimal, in the sense that the nonadiabatic losses are minimized on a level line. To achieve adiabatic passage we have to use a level line satisfying

$$\Delta_1 T_c \gg 1. \tag{32}$$

The appropriate time-dependent chirp is designed from the chosen path in the parameter space and the given pulse envelope.

The path (b) of Fig. 11 connects $|v=0,\tilde{J}=0\rangle$ to $|v=6,\tilde{J}=0\rangle$, which is the final state chosen here. We use a Gaussian

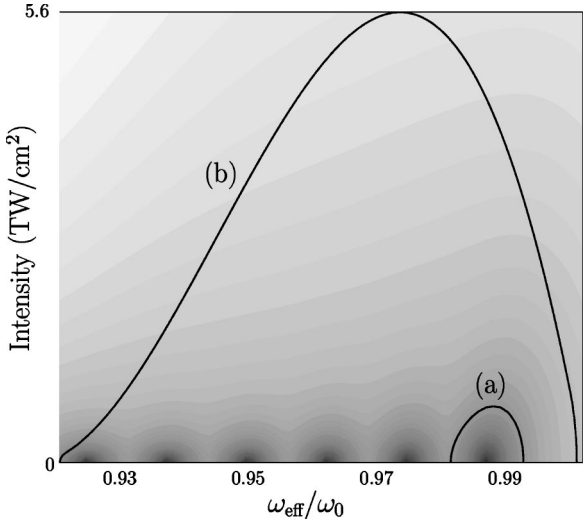


FIG. 11. Contour plot of the difference of the neighboring infrared-laser dressed energy surfaces of the aligned molecule for $\gamma_a=24$ (corresponding to the peak intensity $I_{0a}\approx 8$ TW/cm$^2$ for CO molecules and giving $\langle\cos^2\Theta\rangle\approx 0.79$). Darker zones characterize closer surfaces. Two appropriate paths connecting $|v=0,\tilde{J}=0\rangle$ with, respectively, (a) $|v=1,\tilde{J}=1\rangle$ and (b) $|v=6,\tilde{J}=0\rangle$ are shown.

intensity envelope of full width at half maximum $T_c\approx 4$ ps. We start at the detuning $\Delta_i=1.6\times10^{-4}$ a.u. and end at $\Delta_f=2.1\times10^{-3}$ a.u. The chirp designed from path (b) with the Gaussian envelope has roughly the shape of a hyperbolic tangent curve (see Sec. II C 1, Figs. 3–5). Figure 12 displays the population history with the complete laser sequence: the nanosecond laser (with a Gaussian intensity envelope of full width at half maximum $T_a\approx 0.4$ ns) is first switched on; while it is at its maximum, the chirping laser with the parameters determined above from path (b) is applied and induces transitions among the pendular vibrational states; finally the nanosecond laser is switched off to reconnect the pendular states to the rotational states. The almost complete transfer from $|v=0,J=0\rangle$ to $|v=6,J=0\rangle$ occurs. The figure shows the projections of the time-dependent state on the molecular bare states. This corresponds to a monotonic adiabatic transfer between the two vibrational pendular states involved in the process.

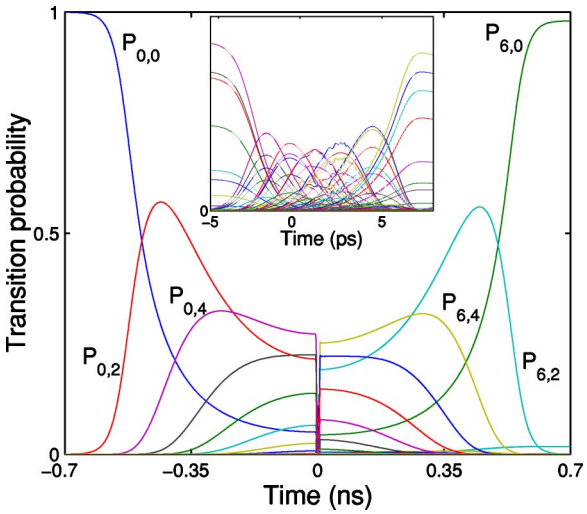


FIG. 12. (Color online) Population history with the peak intensity $I_{0c}=5.6$ TW/cm$^2$ and the chirp designed from the path (b) of Fig. 11: the curves represent the projections $P_{v,J}=|\langle v,J|\psi(t)\rangle|^2$ of the state $\psi(t)$, solution of the time-dependent Schrödinger equation, on the bare molecular states $|v,J\rangle$. The inset displays details of the population history during the picosecond time scale of the chirped laser.

We remark that the process allowing adiabatic passage from $|v=0,J=0\rangle$ to $|v=1,J=1\rangle$ (not shown) leads to a final non-negligible permanent alignment of the molecule with a value of $\langle\cos^2\theta\rangle=0.6$. Adiabatic passage to higher $v$ and $J$ leads to smaller $\langle\cos^2\theta\rangle$ values ($\gtrsim 0.5$).

It is important to note that climbing the rotational ladder while climbing the vibrational one, following the sequence $|v=0,\tilde{J}=0\rangle$, $|v=1,\tilde{J}=3\rangle$, $|v=2,\tilde{J}=4\rangle$, $|v=3,\tilde{J}=7\rangle$, …, i.e., with alternating $\Delta\tilde{J}=1$ and $\Delta\tilde{J}=3$, is theoretically possible but would require a specific nonmonotonic large chirp for this highly anharmonic sequence of $\tilde{J}$.

We remark that we could have also used a multiphoton chirp instead of sequential one-photon steps, but with a nonmonotonic chirp, as explained in the preceding section for the rotationless model.

### D. State selectivity by Raman chirping

The state selective transfer can also be implemented using a Raman process: one of the lasers of the Raman process, of fixed frequency, aligns the molecule and the second laser is chirped to produce the adiabatic passage. We have tested this scheme numerically, choosing a path in parameter space that connects $|v=0,\tilde{J}=0\rangle$ to $|v=6,\tilde{J}=0\rangle$. We have also obtained in this case close to 100% transfer efficiency with $I_{0c}=4.4$ TW/cm$^2$.

One could also achieve efficiently with a nonmonotonic chirp the selective climbing of $v$ and $J$: $|v=0,J=0\rangle\rightarrow|v=1,J=2\rangle\rightarrow|v=2,J=4\rangle\rightarrow\ldots\rightarrow|v,J=2v\rangle$.

## IV. CONCLUSION

We have developed systematic tools to transfer population by adiabatic passage induced by chirped frequencies using quasienergy surfaces as functions of the field parameters. We have shown that, in a realistic model including rotation, the alignment of molecules during a nanosecond laser pulse can be used for an efficient rovibrational state selectivity. In addition to leading the molecule to a given vibrational state, this method offers the possibility to obtain either an isotropic molecule in $J=0$ or a molecule in a well-defined anisotropic $J>0$ state.

## ACKNOWLEDGMENTS

We thank L. P. Yatsenko for stimulating discussions. We acknowledge the financial supports by the *Action Concertée Incitative Photonique* from the French Ministry of Research and by the Conseil Régional de Bourgogne.

[1] J. Karczmarek, J. Wright, P. B. Corkum, and M. Ivanov, Phys. Rev. Lett. **82**, 3420 (1999).
[2] T. Seideman, J. Chem. Phys. **111**, 4397 (1999).
[3] S. Chelkowski, A. D. Bandrauk, and P. B. Corkum, Phys. Rev. Lett. **65**, 2355 (1990).
[4] S. Chelkowski and G. N. Gibson, Phys. Rev. A **52**, R3417 (1995); S. Chelkowski and A. D. Bandrauk, J. Raman Spectrosc. **28**, 459 (1997).
[5] D. J. Maas, C. W. Rella, P. Antoine, E. S. Toma, and L. D. Noordam, Phys. Rev. A **59**, 1374 (1999).
[6] S. Guérin, Phys. Rev. A **56**, 1458 (1997).
[7] K. Drese and M. Holthaus, Eur. Phys. J. D **5**, 119 (1999).
[8] S. Chelkowski and A. D. Bandrauk, J. Chem. Phys. **99**, 4279 (1993).
[9] J. C. Davis and W. S. Warren, J. Chem. Phys. **110**, 4229 (1999).
[10] F. Légaré, S. Chelkowski, and A. D. Bandrauk, Chem. Phys. Lett. **329**, 469 (2000).
[11] I. V. Andrianov and G. K. Paramonov, Phys. Rev. A **59**, 2134 (1999).
[12] S. Sen, S. Ghosh, S. S. Bhattacharyya, and S. Saha, J. Chem. Phys. **116**, 581 (2002).
[13] A. Adelswärd, S. Wallentowitz, and W. Vogel, Phys. Rev. A **67**, 063805 (2003).
[14] B. Friedrich and D. Herschbach, Phys. Rev. Lett. **74**, 4623 (1995).
[15] J. Ortigoso, M. Rodriguez, M. Gupta, and B. Friedrich, J. Chem. Phys. **110**, 3870 (1999).
[16] C. M. Dion, A. Keller, O. Atabek, and A. D. Bandrauk, Phys. Rev. A **59**, 1382 (1999).
[17] T. Seideman, J. Chem. Phys. **115**, 5965 (2001).
[18] S. Guérin and H. R. Jauslin, Adv. Chem. Phys. **125**, 147 (2003).
[19] S. Guérin, L. P. Yatsenko, and H. R. Jauslin, Phys. Rev. A **63**, 031403 (2001).
[20] L. P. Yatsenko, S. Guérin, and H. R. Jauslin, Phys. Rev. A **65**, 043407 (2002).
[21] S. Guérin, R. G. Unanyan, L. P. Yatsenko, and H. R. Jauslin, Phys. Rev. A **66**, 032311 (2002).
[22] S. Guérin, S. Thomas, and H. R. Jauslin, Phys. Rev. A **65**, 023409 (2002).
[23] S. Guérin, F. Monti, J.-M. Dupont, and H. R. Jauslin, J. Phys. A **30**, 7193 (1997).
[24] G. Maroulis, J. Phys. Chem. **100**, 13466 (1996)
[25] B. Broers, H. B. vanLinden van den Heuvell, and L. D. Noordam, Phys. Rev. Lett. **69**, 2062 (1992); P. Balling, D. J. Maas, and L. D. Noordam, Phys. Rev. A **50**, 4276 (1994).
[26] A. Keller, C. M. Dion, and O. Atabek, Phys. Rev. A **61**, 023409 (2000).
[27] S. Guérin, L. P. Yatsenko, H. R. Jauslin, O. Faucher, and B. Lavorel, Phys. Rev. Lett. **88**, 233601 (2002).